Atmos. Chem. Phys. Discuss., 15, 32157–32183, 2015
www.atmos-chem-phys-discuss.net/15/32157/2015/
doi:10.5194/acpd-15-32157-2015

Atmospheric Chemistry and Physics Discussions

Single particle characterization of biomass burning organic aerosol (BBOA): evidence for non-uniform mixing of high molecular weight organics and potassium

A. K. Y. Lee[1], M. D. Willis[1], R. M. Healy[2,3,a], J. M. Wang[3], C.-H. Jeong[3], J. C. Wenger[2], G. J. Evans[3], and J. P. D. Abbatt[1]

[1]Department of Chemistry, University of Toronto, Toronto, Canada
[2]Department of Chemistry and Environmental Research Institute, University College Cork, Ireland
[3]Southern Ontario Centre for Atmospheric Aerosol Research, Department of Chemical Engineering and Applied Chemistry, University of Toronto, Toronto, Canada
[a]now at: Environmental Monitoring and Reporting Branch, Ontario Ministry of the Environment and Climate Change, Toronto, Canada

Received: 27 October 2015 – Accepted: 5 November 2015 – Published: 17 November 2015

Correspondence to: A. K. Y. Lee (alexky.lee@utoronto.ca)

Published by Copernicus Publications on behalf of the European Geosciences Union.

Abstract

Biomass burning is a major source of black carbon (BC) and primary organic aerosol globally. In particular, biomass burning organic aerosol (BBOA) is strongly associated with atmospheric brown carbon (BrC) that absorbs near ultraviolet and visible light, resulting in significant impacts on regional visibility degradation and radiative forcing. The mixing state of BBOA can play a critical role in the prediction of aerosol optical properties. In this work, single particle measurements from a soot-particle aerosol mass spectrometer coupled with a light scattering module (LS-SP-AMS) were performed to examine the mixing state of BBOA, refractory black carbon (rBC) and potassium (K^+, a tracer for biomass burning aerosol) in an air mass influenced by aged biomass burning. Cluster analysis of single particle measurements identified five BBOA-related particle types. rBC accounted for 3–14 w.t. % of these particle types on average. Only one particle type exhibited a strong ion signal for K^+, with mass spectra characterized by low molecular weight organic species. The remaining four particle types were classified based on the apparent molecular weight of the BBOA constituents. Two particle types were associated with low potassium content and significant amounts of high molecular weight (HMW) organic compounds. Our observations indicate non-uniform mixing of particles within a biomass burning plume in terms of molecular weight and illustrate that HMW BBOA can be a key contributor to low-volatility BrC observed in BBOA particles.

1 Introduction

Biomass burning is one of the major global sources of primary particulate matter, contributing approximately 42 and 74 % of global black carbon (BC) and primary organic aerosol, respectively (Bond et al., 2004). Although typical climate forcing calculations only consider BC and dust as light absorbing aerosol components, there is growing evidence that atmospheric brown carbon (BrC, i.e. light-absorbing organic particulate

ACPD
15, 32157–32183, 2015

matter with wavelength-dependent absorption in the ultraviolet-visible spectral region) is strongly associated with biomass burning organic aerosol (BBOA), resulting in significant impacts on regional visibility and radiative forcing (Kirchstetter et al., 2004; Chen and Bond, 2010; Lack et al., 2012, 2013; Saleh et al., 2014; Lu et al., 2015; Washenfelder et al., 2015).

Recent laboratory studies have investigated the physicochemical and optical properties of BrC from biomass burning emissions in order to improve understanding of its climate impacts. McMeeking et al. (2014) performed a series of thermodenuder experiments to examine volatility and absorption properties of laboratory-generated BBOA associated with BC. Compared to the evaporative loss of aerosol mass, lower removal efficiencies of aerosol absorption at the wavelengths of 405 and 532 nm were observed, implying the presence of less volatile, light absorbing BrC in the thermo-processed particles. Saleh et al. (2014) also demonstrated that the effective absorptivity of BrC that was generated from various biomass burning experiments is a function of the black carbon-to-organic aerosol (BC-to-OA) ratio and is largely associated with extremely low-volatility organic compounds (ELVOC) that could not be removed efficiently by a thermodenuder operated at 250 °C. Mohr et al. (2013) recently identified nitrated phenol compounds as potentially important contributors to BrC in BBOA. However, the chemical characteristics of such extremely low-volatility BrC remain largely uncertain.

High molecular weight (HMW) organic compounds can be one of the major contributors to low-volatility BrC in BBOA. A significant number of HMW organic compounds in BBOA have been observed based on different mass spectrometry analyses (e.g. Elias et al., 1999; Smith et al., 2009). More importantly, Dinar et al. (2008) demonstrated that the absorptivity of ambient humic-like substance (HULIS, fulvic acid type) separated from BBOA extracts was enhanced with increasing molecular weight (from 340 to 460 Da), and thus decreasing aerosol volatility. Sun et al. (2007) also reported that the molecular structures of organic compounds that result in absorption spectra similar to that of atmospheric BrC are generally highly oxygenated molecules with more than 18 carbon atoms.

ACPD
15, 32157–32183, 2015

Co-emission of BC and BBOA from biomass burning sources can lead to internal mixing of these components. Internal mixtures of organic, BC and potassium salts in different degree have been observed in biomass burning aerosol using electron microscopic techniques (Li et al., 2003). Due to analytical challenges in single particle characterization, there is limited knowledge of the mixing state of HMW organic compounds in BBOA. Our recent field studies have successfully demonstrated that a soot-particle aerosol mass spectrometer (Aerodyne Research Inc., Billerica, MA) equipped with a light scattering module (LS-SP-AMS) can quantify the mixing state of refractory black carbon (rBC) and organic aerosol in urban environments on a single particle basis (Lee et al., 2015; Willis et al., 2015). Here, we extend the application of this single particle measurement technique to investigate the mixing state of BBOA and other co-emitted species. The primary objective of this study is to investigate the mixing state of potassium (K^+, a tracer of BBOA), rBC and BBOA from a wildfire episode in which emissions were transported from Northern Quebec to Toronto. Note that atmospheric processing can modify mixing state of aerosol particles so that our observation may not reflects the mixing state of freshly emitted biomass burning aerosol. Compared to the results from thermodenuder experiments, the LS-SP-AMS measurements provide chemical insight into further our understanding of the observed volatility and optical properties of biomass burning particles.

2 Experiment

2.1 Sampling detail and instrumentation

Measurements were performed at the Southern Ontario Centre for Atmospheric Aerosol Research Facility, located in downtown Toronto (43.66° N, 79.40° W). The sampling period was 12–17 June 2013, and encompassed an air mass heavily influenced by biomass burning (14 June, 14:00 to 16 June, 11:00 LT – local time) attributed to wildfire events in Quebec (Healy et al., 2015; Willis et al., 2015). The biomass burning

ACPD
15, 32157–32183, 2015

influenced air mass took approximately 2 days transporting from Quebec to Toronto based on back trajectory analysis (Hybrid Single-Particle Lagrangian Integrated Trajectory (HYSPLIT) Model). All instruments were connected to a common sampling line (a 10 cm inner diameter stainless steel tube) with a total flow rate of 170 L min^{-1}. The stainless steel sampling line was connected to a 2.5 µm cut-off inlet, located 15 m from the roadside and 3 m above ground level.

A soot-particle aerosol mass spectrometer (Aerodyne Research Inc., Billerica, MA) equipped with a light scattering module (LS-SP-AMS) was the key instrument for this analysis (see Sects. 2.2–2.3). Other co-located aerosol instruments included an aerosol time-of-flight mass spectrometer (ATOFMS 3800, TSI Inc., Shoreview, MN), a photoacoustic soot spectrometer (PASS-3, Droplet Measurement Techniques, Boulder, CO), an aerosol chemical speciation monitor (ACSM, Aerodyne Research Inc., Billerica, MA) and a scanning mobility particle sizer (SMPS, Model 3936N76, TSI Inc., Shoreview, MN). The ACSM was used to quantify the ambient mass concentration of non-refractory particulate matter (NR-PM) (Ng et al., 2011) with a time resolution of 30 min in this study (see details in the Supplement). A thermodenuder (Dekati Inc., Finland) operated at 250 °C with a flow rate of 6 L min^{-1}, was used to remove coating materials associated with rBC particles. The residence time for particles in the heated section of the thermodenuder was 1.9 s and the particle transmission efficiency was approximately 72 % (Healy et al., 2015). The PASS-3 and SMPS switched between sampling ambient aerosol and denuded aerosol every 10 min using an automated sampling valve. The details of ATOFMS, PASS-3 and thermodenuder for this field campaign have been reported in Healy et al. (2015).

2.2 Soot particle aerosol mass spectrometer

A LS-SP-AMS was used to investigate the mixing state of rBC-containing particles on a single particle basis. The working principle of the LS-SP-AMS has been reported elsewhere (Onasch et al., 2012; Lee et al., 2015). In brief, rBC-containing particles are vaporized at ~ 4000 K by a 1064 nm continuous wave intracavity infrared laser similar

ACPD
15, 32157–32183, 2015

to that of the single particle soot photometer (SP2, Droplet Measurement Technologies) (Onasch et al., 2012). The resulting vapour is ionized via 70 eV electron impact and then detected by a high-resolution time-of-flight mass spectrometer operated in *V* mode, which provides a mass resolving power of ~ 2000 at m/z 28 (DeCarlo et al., 2006; Canagaratna et al., 2007). A resistively heated tungsten vaporizer was removed from our instrument so that only rBC and its coating materials were detected (Massoli et al., 2015; Willis et al., 2015). A single slit chopper with ~ 2 % throughput was used. The LS-SP-AMS was operated at one-minute time resolution alternating between bulk mass spectrum (MS), particle time-of-flight (pToF) and single particle modes throughout the study.

Direct calibration of the ionization efficiency for nitrate (IE_{NO_3}) is not possible without the tungsten vaporizer. Before removal of the tungsten vaporizer from the LS-SP-AMS, ammonium nitrate (NH_4NO_3) particles generated by a constant output atomizer (TSI Inc., Model 3076) were dried using a diffusion dryer, and subsequently size-selected at 300 nm using a differential mobility analyzer (DMA, TSI Inc., Model 3081) for determining the mass-based ionization efficiency of nitrate (mIE_{NO_3}). Similarly, the LS-SP-AMS was calibrated for rBC quantification using dried 300 nm Regal Black particles (Regal 400R Pigment Black, Cabot Corp.), a calibration standard recommended by Onasch et al. (2012) to determine the mass-based ionization efficiency of rBC (mIE_{rBC}). The mass of individual dried 300 nm Regal Black particles was ~ 11.2 fg based on aerosol particle mass analyzer measurements (APM model 3600, Kanomax Inc.) (Willis et al., 2014). The relative ionization efficiency of rBC ($RIE_{rBC} = mIE_{rBC}/mIE_{NO_3}$) was 0.2 ± 0.05 (1σ uncertainty). Assuming that RIE_{rBC} remains unchanged, mIE_{NO_3} and IE_{NO_3} were calculated based on measured values of mIE_{rBC} (after removing the tungsten vaporizer) and the known RIE_{rBC}. The average of the calculated mIE_{rBC} values was 189 ± 20 ions pg^{-1} based on four independent calibrations performed throughout the study. The calculated IE_{NO_3} was then used with recommended RIE values (Jimenez et al., 2003, i.e. nitrate = 1.1, sulfate = 1.2, organics = 1.4 and ammonium = 4) to quantify non-refractory aerosol species associated

ACPD
15, 32157–32183, 2015

with rBC (referred to as NR-PM_{rBC}). Note that our previous studies have shown that the uncertainties of the recommended RIE for NR-PM_{rBC} for the SP-AMS can be up to 50 % (Willis et al., 2014; Lee et al., 2015).

The ensemble MS and pToF data were processed using the AMS data analysis software (Squirrel, version 1.51H for unit mass resolution (UMR) data and Pika, version 1.10H for high resolution peak fitting, http://cires.colorado.edu/jimenez-group/ToFAMSResources/ToFSoftware/index.html) with the corrected air fragment column of the standard fragmentation table (Allan et al., 2004; DeCarlo et al., 2006). Signals for rBC were quantified by the sum of carbon ion clusters (C_x^+, i.e. C_1^+–C_9^+) using high-resolution mass spectral data. The average C_1^+ to C_3^+ ratio (0.6) obtained from Regal Black calibration was used to correct the interference in C_1^+ from the non-refractory organics in ambient aerosol. Collection efficiency (CE) for rBC particles was determined in this study using beam width probe measurements described previously (Willis et al., 2014). Ambient rBC-containing particles had an average beam width (σ) = 0.46 ± 0.03 mm, and hence a CE of 0.6 was applied for absolute quantification of rBC and NR-PM_{rBC} (Willis et al., 2014). The CE applied does not impact calculations of mass fraction of rBC (mf_{rBC}) in the rBC-containing particles. Positive matrix factorization (PMF) analysis that covered a wider range of the sampling period (i.e. 31 May–17 June 2015) was performed in our previous work to investigate the potential sources and characteristics of organic aerosol (Willis et al., 2015) and thus is not described further here.

2.3 Single particle measurements and data analysis

The design and working principles of the LS module installed in different versions of the AMS have been previously described in detail (Cross et al., 2009; Freutel et al., 2013; Liu et al., 2013; Lee et al., 2015). The LS module consists of a 405 nm continuous wave laser (CrystaLaser, LC BCL-050-405) that overlaps perpendicularly and completely with the particle beam ~ 0.265 m downstream of the chopper (Cross et al., 2007). Scattered light from sampled particles is collected using an ellipsoidal mirror

ACPD
15, 32157–32183, 2015

and detected with a photomultiplier tube (PMT). A LS signal can be obtained if a sampled particle is larger than the optical detection limit. The 50 % cut-off mobility diameter (d_m) (i.e. a diameter that represents 50 % counting efficiency of particle number when compared to a condensation particle counter) of the LS module determined using dried NH_4NO_3 particles is ~ 250 nm, which is approximately equal to a vacuum aerodynamic diameter (d_{va}) of ~ 340 nm (the density and shape factor of NH_4NO_3 particles are 1.72 g cm^{-3} and 0.8, respectively). Once a light scattering signal is detected, the computer is triggered to save the whole pToF trace, from which the single particle mass spectrum is subsequently obtained.

Single particle measurements were analyzed based on a particle categorization procedure, fragmentation table modification and *k* means clustering algorithm described previously (Lee et al., 2015), except that *m*/*z* 39 (K^+) was also included in the cluster analysis. Note that the tungsten vaporizer was removed from the LS-SP-AMS, and hence the instrumental background for K^+ predominantly due to surface ionization on the tungsten vaporizer was minimal. LS signals and single particle mass spectra with unit mass resolution (UMR) were processed using the AMS LS data processing software (Sparrow, version1.04E, http://cires.colorado.edu/jimenez-group/ToFAMSResources/ToFSoftware/index.html). The built-in *k* means clustering algorithm in IGOR Pro (WaveMetrics Inc., version 6.2.2.2) was used to analyze single particle data for up to 25 clusters (Lee et al., 2015). Multiple clusters were manually merged into final particle classes if they exhibited similar mass spectral features and size distributions. Note that *k* means clustering has been extensively applied to analyze single particle data measured from the ATOFMS (Rebotier and Prather, 2007; Friedman et al., 2009; Giorio et al., 2012; Gross et al., 2010; Healy et al., 2010, 2013; Pagels et al., 2013) and the results are highly consistent with other clustering algorithms such as ART-2a and hierarchical clustering (Rebotier and Prather, 2007; Giorio et al., 2012).

ACPD
15, 32157–32183, 2015

3 Results and discussion

3.1 Observations of biomass burning influenced air mass

A high loading of rBC-associated organics (referred to as Org_{rBC}) was observed during a period of strong biomass burning influence due to transported wildfire emissions originating from Quebec (Fig. 1a, 14 June, 14:00 LT to 16 June, 11:00 LT, referred to as "BB period") (Healy et al., 2015). Potassium (K^+, a tracer of BBOA) measured by the LS-SP-AMS is in good agreement with the K-containing particle number counts measured by the ATOFMS, and is strongly correlated with increased levels of Org_{rBC} (Fig. 1a–c), indicating a significant contribution of BBOA to the total Org_{rBC} during the BB period. This is in good agreement with results of a PMF analysis, which indicate that a PMF-BBOA factor correlates well with K^+ (Fig. 1b) (Willis et al., 2015). The average mass fractions of m/z 60 (a marker ion for BBOA) and 44 to total organic (f_{60} and f_{44}) during the BB period were 0.013 and 0.09, respectively, which is consistent with previous field observations for BBOA (Cubison et al., 2011). Even though K^+ and Org_{rBC} observed within the BB period likely have the same origin, different peak positions in K^+ and Org_{rBC} size distributions suggest non-uniform mixing of these two aerosol components in biomass burning emissions (Fig. 1d).

3.2 Single particle observations – BBOA particle types

Cluster analysis of LS-SP-AMS single particle mass spectra was performed to investigate the mixing states of K^+, Org_{rBC} and rBC, yielding nice distinct particle classes (Table 1). Approximately 90 % of the particles were classified into five BBOA-related particle types, namely BBOA-K, BBOA-1, BBOA-2, BBOA-3, and BBOA-4 (see discussion below). rBC was only a minor constituent of these particle classes (mf_{rBC} = 0.03–0.14), which is agreement with the PMF-BBOA factor reported in Willis et al. (2015). Assuming a core-shell structure and spherical particle morphology, we estimate that rBC cores of most BBOA particle types were thickly coated by organic species (Fig. S1

ACPD
15, 32157–32183, 2015

in the Supplement). For example, a 320 nm BBOA particle (i.e. $d_{va} \sim 400$ nm, assuming the effective density of rBC and BBOA are 0.8 and 1.3 g cm^{-3}, respectively) that consists of 5 % of rBC by mass would have a BC core of radius ~ 68 nm covered by ~ 92 nm of BBOA material.

An rBC-rich particle type with mf_{rBC} of ~ 0.8–0.9 was identified in our previous observations in downtown Toronto likely arising from fresh traffic exhaust (Lee et al., 2015; Willis et al., 2015). rBC-rich particles accounted for only about 1 % of the total particles detected during this biomass burning episode, in part due to the lower cut-off size limitation of the LS module (Lee et al., 2015). Also, a particle class associated with a high mass fraction of hydrocarbon-like organic aerosol materials (HOA-rich particle class reported in Lee et al., 2015 and Willis et al., 2015) was not observed during this period. It is possible that the LS-SP-AMS actually detected a small number of HOA-rich particles during the BB period but cluster analysis could not separate them from the more dominant BBOA particle classes due to similar mass spectral characteristics. Accumulation mode SO_4-rich (3 %) and NO_3-rich (5 %) particle classes with low rBC content ($mf_{rBC} < 0.02$) were also identified, similar to our previous observations in downtown Toronto (Lee et al., 2015).

3.3 Mixing of K^+ in BBOA

The five BBOA-related particle classes give relatively strong total ion signals within the BB period as illustrated in Fig. 1c, which is in good agreement with the PMF-BBOA factor and K^+ (Fig. 1b). Figure 2 demonstrates the average mass spectra (grey and green trace) of each BBOA-related particle class and the mass spectral histograms (normalized to the number of particles in each particle class, red trace) that show the relative frequency of a signal at each m/z. Only one particle type, BBOA-K, exhibits a strong ion signal for K^+ (m/z 39) with mass spectra characterized by low molecular weight organic fragment ions (Fig. 2a). The ion fraction of m/z 39 for BBOA-K and other BBOA-related particle classes are 0.33 and less than 0.02, respectively (Fig. 3 and Table 1). The inset in Fig. 3 presents the ion fraction distribution of m/z 39 for

ACPD
15, 32157–32183, 2015

BBOA-K (ranging from 0.1 to 0.8). Furthermore, ternary diagrams illustrate the relative abundance of K^+, rBC and organic ion signals in each BBOA-related particle type (Fig. 4).

These observations highlight that (1) K^+ is not uniformly mixed in BBOA although it has been extensively used as a tracer for BBOA, and (2) a large number fraction of BBOA particles are characterized by low K^+ and rBC content. Assuming that the relative ionization efficiency of K^+ (RIE_K) is equal to 2.9 (Drewnick et al., 2006), the average mass fractions of K^+ for BBOA-K and the other BBOA-related particle types are approximately 20 % and < 1 %, respectively. While BBOA-K accounted for ~ 15 % of the detected particle number (Table 1), our complementary ATOFMS measurements revealed that particles with a strong K^+ signal accounted for over 60 % of the detected particle number for the same period. However, ATOFMS is highly sensitive towards K^+ (Gross et al., 2000), thus even particles with low potassium mass content can exhibit high relative positive ion intensities for K^+. It is also important to note that ATOFMS and LS-SP-AMS cannot detect BBOA particles that are without any components absorbing at a wavelength of 266 nm and in the absence of rBC, respectively. A direct comparison between the two measurements is not straightforward as the mass quantifications of K^+ at the single particle level for both instruments remain highly uncertain.

3.4 Mixing of high molecular weight organic compounds in BBOA

The remaining four BBOA particle types were classified according to the apparent molecular weight of BBOA constituents (Fig. 2b–e). The average value of f_{60} for BBOA-4 (0.004) is smaller than those of other BBOA particle types (ranging from 0.008 to 0.015). Note that m/z 44 (a tracer ion for organic acids) is the main contributor to BBOA-4, whereas other BBOA particle types are dominated by ions at m/z 29 and 43, suggesting that BBOA-4 is more oxidized relative to other BBOA particles. Figure 5a illustrates the normalized cumulative histograms of mass-to-charge ratios (from m/z 12 to 628, excluding m/z 39 and fragments with strong interferences from air and ammonium, see Lee et al., 2015) for each BBOA particle class, all BBOA parti-

ACPD
15, 32157–32183, 2015

cle types and ensemble Org_{rBC} within the BB period. Two particle types, BBOA-3 and BBOA-4, are associated with significant amounts of HMW organic fragments (i.e. more than 50 % of the ion signal arose from organic fragments at m/z 100 or larger). For BBOA-2, ∼ 23 % of the ion signal resides in HMW organic fragments. BBOA-K and BBOA-1 are mainly composed of low molecular weight organics with over 96 % of their ion signal arising from organic fragments smaller than m/z 100. Further, a significant number of observed BBOA particles are composed of HMW organic fragments, up to 80 % by mass (Fig. 5b). These observations demonstrate that (1) the mixing state of BBOA is not uniform in terms of organic molecular weight, and (2) a large number fraction of BBOA single particle mass spectra (∼ 40 %) has major contributions from HMW organic fragment ions, which are detected even though a hard ionization technique (electron impact) was used in the LS-SP-AMS.

HMW mass spectral signatures, some of which are associated with polycyclic aromatic hydrocarbons, were also observed in the ATOFMS data for the same period (see Fig. S4 for the average ATOFMS mass spectrum). However, those spectra only accounted for ∼ 0.5 % of the total number of spectra detected by the ATOFMS during the BB period. Even though the ATOFMS has been previously demonstrated to detect HMW oligomeric species in both ambient air and chamber experiments (Gross et al., 2006; Denkenberger et al., 2007; Healy et al., 2010), its sensitivity towards HMW organics may be influenced by chemical matrix effects, making the detection and quantification of HMW organics in ambient particles challenging (Reilly et al., 2000).

Although the ensemble size distributions of K^+ and Org_{rBC} are observably different (Fig. 1d), the size distributions of BBOA-K and other BBOA-related particle classes are similar to each other except that BBOA-4 peaks at a slightly larger particle diameter (the insets in Fig. 2a–e), likely due to measurement bias of the LS module towards larger particle sizes (Lee et al., 2015). Nevertheless, it is worth nothing that there is no significant difference between the ensemble size distributions of low ($< m/z$ 100) and high ($> m/z$ 100) molecular weight organics (Fig. 1d). This suggests that ensemble size distributions are insufficient to visualize external mixing of the BBOA particle types

ACPD
15, 32157–32183, 2015

with different average molecular weight, and also highlights the relevance and unique capabilities of single particle mass spectrometry observations.

3.5 Volatility and optical properties of BBOA

To assess the volatility of BBOA, the mass fraction of total BBOA, regardless of rBC content, retained in thermo-processed particles was estimated based on the SMPS and ACSM measurements (see details in Supplement). The removal efficiency of aerosol volume, based on SMPS measurements, was 60–80 % for the majority of the sampling period and decreased to ~ 40 % on 15 June, when the site was most heavily impacted by the wildfire emissions (Fig. S2a). The estimation based on ACSM measurements also illustrates that approximately 60 % of the total BBOA was retained in the thermo-denuded particles on 15 June to match the SMPS observations, given the fact that BBOA dominated the total aerosol mass on 15 June (Fig. S2b, see details in Supplement). Furthermore, a strong correlation between the thermo-denuded SMPS aerosol volume (equivalent to aerosol mass if particle density is relatively constant) and the estimated low-volatility aerosol mass is observed for the entire sampling period (R^2 = 0.93, blue open circles in Fig. 6a) when all rBC and ~ 60 % of the total BBOA is assumed to remain after the thermodenuder. It is clear that rBC mass alone cannot explain the observed aerosol volatility (R^2 = 0.31, black solid circles in Fig. 6a). The above observations indicate the presence of low-volatility BBOA materials.

The absorption of thermo-denuded aerosol at a wavelength of 405 nm (B_{abs}) was measured by the PASS-3 (Figs. S2d and 6b). Similar to the case of aerosol volatility, the strong absorption characteristics observed during the BB period cannot be explained by the presence of rBC alone, because the rBC loading was roughly constant throughout the sampling period (R^2 = 0.33, black solid circles in Fig. 6b). The correlation between thermo-denuded particles and aerosol absorption at 405 nm is improved significantly if low-volatility BBOA (60 % of the total BBOA) is included in the calculation (R^2 = 0.84, blue open circles in Fig. 6b). Our previous work reported that absorption enhancement attributable to lensing at 781 nm was not observed for rBC

ACPD
15, 32157–32183, 2015

during the BB period based on the PASS-3 measurement (Healy et al., 2015). Furthermore, a recent study has reported that the interference on absorption measurement due to pyrolyzed ambient organic aerosol in thermodenuder operated at 250 °C is minimal (Liu et al., 2015). Therefore, these observations suggest that low-volatility BBOA components could be a key contributor to BrC in the thermo-denuded particles. The ion fractions of BBOA-2, BBOA-3 and BBOA-4 from the single particle measurements accounted for ~ 61 % of the total ion signal, which is equivalent to mass as most of the observed BBOA particles are dominated by organics, from all BBOA-related particle classes during the BB period. This implies that medium to high molecular weight organic compounds may contribute significantly to low-volatility BrC in the biomass burning affected atmosphere.

4 Conclusions and atmospheric implications

This is the first study to quantify the mixing state of BBOA, K^+ and rBC in ambient biomass burning aerosol using the LS-SP-AMS. BBOA-related particle types are composed of low rBC mass (mf_{rBC} = 0.03–0.14). Even though K^+ has been considered as a tracer of BBOA, our results demonstrate that K^+ is not uniformly mixed in BBOA and that over 80 % of BBOA particles observed here are characterised by low K^+ content (i.e. < 1 w.t. % by assuming RIE_K of 2.9). High molecular weight organic compounds were clearly observed in some BBOA particles. A large fraction of BBOA particles (BBOA-3 and BBOA-4) detected in this study are composed of HMW organic compounds with low rBC and K^+ content.

Thermodenuder experiments indicate the presence of low-volatility BrC in BBOA. Based on SMPS and aerosol mass spectrometry measurements, we estimated that about 60 % of the total BBOA mass was retained in the thermo-processed particles. This is consistent with recent observations which demonstrated that laboratory-generated BBOA particles could be composed of extremely low-volatility BrC depending on the burning conditions (Saleh et al., 2014). Liu et al. (2015) also observed low-

ACPD
15, 32157–32183, 2015

volatility secondary BrC that associated with large rBC particles in wintertime UK. Notably, BBOA-2, BBOA-3 and BBOA-4 accounted for ~ 61 % of ion signals from BBOA-related particle classes during the BB period, highlighting that medium to high molecular weight organic compounds may contribute significantly to low-volatility BrC. The observed non-uniform mixing state of BBOA in terms of molecular weight also suggests that it may be inappropriate to assume uniform distributions of aerosol volatility and absorption for BBOA particles.

The Supplement related to this article is available online at doi:10.5194/acpd-15-32157-2015-supplement.

Acknowledgement. This work was financially supported by Natural Sciences and Engineering Research Council (NSERC) of Canada, the Canada Foundation for Innovation and the Marie Curie Action FP7-PEOPLE-IOF-2011 (Project: CHEMBC, No. 299755).

References

Allan, J., Delia, A., Coe, H., Bower, K., Alfarra, M., Jimenez, J., Middlebrook, A., Drewnick, F., Onasch, T., Canagaratna, M., Jayne, J., and Worsnop, D.: A generalised method for the extraction of chemically resolved mass spectra from aerodyne aerosol mass spectrometer data, J. Aerosol Sci., 35, 909–922, 2004.

Bond, T. C., Streets, D. G., Yarber, K. F., Nelson, S. M., Woo, J. H., and Klimont, Z.: A technology-based global inventory of black and organic carbon emissions from combustion, J. Geophys. Res.-Atmos., 109, D14203, doi:10.1029/2003JD003697, 2004.

Canagaratna, M. R., Jayne, J. T., Jimenez, J. L., Allan, J. D., Alfarra, M. R., Zhang, Q., Onasch, T. B., Drewnick, F., Coe, H., Middlebrook, A., Delia, A., Williams, L. R., Trimborn, A. M., Northway, M. J., DeCarlo, P. F., Kolb, C. E., Davidovits, P., and Worsnop, D. R.: Chemical and microphysical characterization of ambient aerosols with the aerodyne aerosol mass spectrometer, Mass Spectrom. Rev., 26, 185–222, 2007.

ACPD
15, 32157–32183, 2015

Denkenberger, K. A., Moffet, R. C., Holecek, J. C., Rebotier, T. P., and Prather, K. A.: Real-time, single-particle measurements of oligomers in aged ambient aerosol particles, Environ. Sci. Technol., 41, 5439–5446, 2007.

Chen, Y. and Bond, T. C.: Light absorption by organic carbon from wood combustion, Atmos. Chem. Phys., 10, 1773–1787, doi:10.5194/acp-10-1773-2010, 2010.

Cross, E. S., Slowik, J. G., Davidovits, P., Allan, J. D., Worsnop, D. R., Jayne, J. T., Lewis, D. K., Canagaratna, M., and Onasch, T. B.: Laboratory and ambient particle density determinations using light scattering in conjunction with aerosol mass spectrometry, Aerosol Sci. Tech., 41, 343–359, 2007.

Cross, E. S., Onasch, T. B., Canagaratna, M., Jayne, J. T., Kimmel, J., Yu, X.-Y., Alexander, M. L., Worsnop, D. R., and Davidovits, P.: Single particle characterization using a light scattering module coupled to a time-of-flight aerosol mass spectrometer, Atmos. Chem. Phys., 9, 7769–7793, doi:10.5194/acp-9-7769-2009, 2009.

Cubison, M. J., Ortega, A. M., Hayes, P. L., Farmer, D. K., Day, D., Lechner, M. J., Brune, W. H., Apel, E., Diskin, G. S., Fisher, J. A., Fuelberg, H. E., Hecobian, A., Knapp, D. J., Mikoviny, T., Riemer, D., Sachse, G. W., Sessions, W., Weber, R. J., Weinheimer, A. J., Wisthaler, A., and Jimenez, J. L.: Effects of aging on organic aerosol from open biomass burning smoke in aircraft and laboratory studies, Atmos. Chem. Phys., 11, 12049–12064, doi:10.5194/acp-11-12049-2011, 2011.

DeCarlo, P. F., Kimmel, J. R., Trimborn, A., Northway, M. J., Jayne, J. T., Aiken, A. C., Gonin, M., Fuhrer, K., Horvath, T., Docherty, K. S., Worsnop, D. R., and Jimenez, J. L.: Field-deployable, high-resolution, time-of-flight aerosol mass spectrometer, Anal. Chem., 78, 8281–8289, 2006.

Dinar, E., Riziq, A. A., Spindler, C., Erlick, C., Kiss, G., and Rudich, Y.: The complex refractive index of atmospheric and model humic-like substances (HULIS) retrieved by a cavity ring down aerosol spectrometer (CRD-AS), Faraday Discuss., 137, 279–295, 2008.

Drewnick, F., Hings, S. S., Curtius, J., Eerdekens, G., and Williams, J.: Measurement of fine particulate and gas-phase species during the New Year's fireworks 2005 in Mainz, Germany, Atmos. Environ., 40, 4316–4327, 2006.

Elias, V. O., Simoneit, B. R. T., Pereira, A. S., Cabral, J. A., and Cardoso, J. N.: Detection of high molecular weight organic tracers in vegetation smoke samples by high-temperature gas chromatography-mass spectrometry, Environ. Sci. Technol., 33, 2369–2376, 1999.

ACPD
15, 32157–32183, 2015

Freutel, F., Drewnick, F., Schneider, J., Klimach, T., and Borrmann, S.: Quantitative single-particle analysis with the Aerodyne aerosol mass spectrometer: development of a new classification algorithm and its application to field data, Atmos. Meas. Tech., 6, 3131–3145, doi:10.5194/amt-6-3131-2013, 2013.

Friedman, B., Herich, H., Kammermann, L., Gross, D. S., Arneth, A., Holst, T., and Cziczo, D. J.: Subarctic atmospheric aerosol composition: 1. Ambient aerosol characterization, J. Geophys. Res.-Atmos., 114, D13203, doi:10.1029/2009JD011772, 2009.

Giorio, C., Tapparo, A., Dall'Osto, M., Harrison, R. M., Beddows, D. C. S., Di Marco, C., and Nemitz, E.: Comparison of three techniques for analysis of data from an aerosol time-of-flight mass spectrometer, Atmos. Environ., 61, 316–326, 2012.

Gross, D. S., Galli, M. E., Silva, P. J., and Prather, K. A.: Relative sensitivity factors for alkali metal and ammonium cations in single particle aerosol time-of-flight mass spectra, Anal. Chem., 72, 416–422, 2000.

Gross, D. S., Galli, M. E., Kalberer, M., Prevot, A. S. H., Dommen, J., Alfarra, M. R., Duplissy, J., Gaeggeler, K., Gascho, A., Metzger, A., and Baltensperger, U.: Real-time measurement of oligomeric species in secondary organic aerosol with the aerosol time-of-flight mass spectrometer, Anal. Chem., 78, 2130–2137, 2006.

Gross, D. S., Atlas, R., Rzeszotarski, J., Turetsky, E., Christensen, J., Benzaid, S., Olson, J., Smith, T., Steinberg, L., Sulman, J., Ritz, A., Anderson, B., Nelson, C., Musicant, D. R., Chen, L., Snyder, D. C., and Schauer, J. J.: Environmental chemistry through intelligent atmospheric data analysis, Environ. Modell. Softw., 25, 760–769, 2010.

Healy, R. M., Hellebust, S., Kourtchev, I., Allanic, A., O'Connor, I. P., Bell, J. M., Healy, D. A., Sodeau, J. R., and Wenger, J. C.: Source apportionment of $PM_{2.5}$ in Cork Harbour, Ireland using a combination of single particle mass spectrometry and quantitative semi-continuous measurements, Atmos. Chem. Phys., 10, 9593–9613, doi:10.5194/acp-10-9593-2010, 2010.

Healy, R. M., Sciare, J., Poulain, L., Crippa, M., Wiedensohler, A., Prévôt, A. S. H., Baltensperger, U., Sarda-Estève, R., McGuire, M. L., Jeong, C.-H., McGillicuddy, E., O'Connor, I. P., Sodeau, J. R., Evans, G. J., and Wenger, J. C.: Quantitative determination of carbonaceous particle mixing state in Paris using single-particle mass spectrometer and aerosol mass spectrometer measurements, Atmos. Chem. Phys., 13, 9479–9496, doi:10.5194/acp-13-9479-2013, 2013.

ACPD
15, 32157–32183, 2015

Healy, R. M., Wang, J. M., Jeong, C., Lee, A. K. Y., Willis, M. D., Jaroudi, E., Zimmerman, N., Hilker, N., Murphy, M., Eckhardt, S., Stohl, A., Abbatt, J. P. D., Wenger, J. C., and Evans, G. J.: Light-absorbing properties of ambient black carbon and brown carbon from fossil fuel and biomass burning sources, J. Geophys. Res.-Atmos., 120, 6619–6633, 2015.

Jimenez, J. L., Jayne, J. T., Shi, Q., Kolb, C. E., Worsnop, D. R., Yourshaw, I., Seinfeld, J. H., Flagan, R. C., Zhang, X. F., Smith, K. A., Morris, J. W., and Davidovits, P.: Ambient aerosol sampling using the aerodyne aerosol mass spectrometer, J. Geophys. Res.-Atmos., 108, 8425, doi:10.1029/2001JD001213, 2003.

Kirchstetter, T. W., Novakov, T., and Hobbs, P. V.: Evidence that the spectral dependence of light absorption by aerosols is affected by organic carbon, J. Geophys. Res.-Atmos., 109, D21208, doi:10.1029/2004JD004999, 2004.

Lack, D. A., Langridge, J. M., Bahreini, R., Cappa, C. D., Middlebrook, A. M., and Schwarz, J. P.: Brown carbon and internal mixing in biomass burning particles, P. Natl. Acad. Sci. USA, 109, 14802–14807, 2012.

Lack, D. A., Bahreini, R., Langridge, J. M., Gilman, J. B., and Middlebrook, A. M.: Brown carbon absorption linked to organic mass tracers in biomass burning particles, Atmos. Chem. Phys., 13, 2415–2422, doi:10.5194/acp-13-2415-2013, 2013.

Lee, A. K. Y., Willis, M. D., Healy, R. M., Onasch, T. B., and Abbatt, J. P. D.: Mixing state of carbonaceous aerosol in an urban environment: single particle characterization using the soot particle aerosol mass spectrometer (SP-AMS), Atmos. Chem. Phys., 15, 1823–1841, doi:10.5194/acp-15-1823-2015, 2015.

Li, J., Posfai, M., Hobbs, P. V., and Buseck, P. R.: Individual aerosol particles from biomass burning in southern Africa: 2, Compositions and aging of inorganic particles, J. Geophys. Res.-Atmos., 108, 8484, doi:10.1029/2002JD002310, 2003.

Liu, S., Russell, L. M., Sueper, D. T., and Onasch, T. B.: Organic particle types by single-particle measurements using a time-of-flight aerosol mass spectrometer coupled with a light scattering module, Atmos. Meas. Tech., 6, 187–197, doi:10.5194/amt-6-187-2013, 2013.

Liu, S., Aiken, A. C., Gorkowski, K., Dubey, M. K., Cappa, C. D., Williams, L. R., Herndon, S. C., Massoli, P., Fortner, E. C., Chhabra, P. S., Brooks, W. A., Onasch, T. B., Jayne, J. T., Worsnop, D. R., China, S., Sharma, N., Mazzoleni, C., Xu, L., Ng, N. L., Liu, D., Allan, J. D., Lee, J. D., Fleming, Z. L., Mohr, C., Zotter, P., Szidat, S., and Prevot, A. S. H.: Enhanced light absorption by mixed source black and brown carbon particles in UK winter, Nat. Commun., 6, 8435–8435, 2015.

ACPD
15, 32157–32183, 2015

Lu, Z., Streets, D. G., Winijkul, E., Yan, F., Chen, Y., Bond, T. C., Feng, Y., Dubey, M. K., Liu, S., Pinto, J. P., and Carmichael, G. R.: Light absorption properties and radiative effects of primary organic aerosol emissions, Environ. Sci. Technol., 49, 4868–4877, 2015.

Massoli, P., Onasch, T. B., Cappa, C. D., Nuamaan, I., Hakala, J., Hayden, K., Li, S., Sueper, D. T., Bates, T. S., Quinn, P. K., Jayne, J. T., and Worsnop, D. R.: Characterization of black carbon-containing particles from soot particle aerosol mass spectrometer measurements on the R/V Atlantis during CalNex 2010, J. Geophys. Res.-Atmos., 120, 2575–2593, 2015.

McMeeking, G. R., Fortner, E., Onasch, T. B., Taylor, J. W., Flynn, M., Coe, H., and Kreidenweis, S. M.: Impacts of nonrefractory material on light absorption by aerosols emitted from biomass burning, J. Geophys. Res.-Atmos., 119, 12272–12286, 2014.

Mohr, C., Lopez-Hilfiker, F. D., Zotter, P., Prevot, A. S. H., Xu, L., Ng, N. L., Herndon, S. C., Williams, L. R., Franklin, J. P., Zahniser, M. S., Worsnop, D. R., Knighton, W. B., Aiken, A. C., Gorkowski, K. J., Dubey, M. K., Allan, J. D., and Thornton, J. A.: Contribution of nitrated phenols to wood burning brown carbon light absorption in Detling, United Kingdom during winter time, Environ. Sci. Technol., 47, 6316–6324, 2013.

Ng, N. L., Herndon, S. C., Trimborn, A., Canagaratna, M. R., Croteau, P. L., Onasch, T. B., Sueper, D., Worsnop, D. R., Zhang, Q., Sun, Y. L., and Jayne, J. T.: An Aerosol Chemical Speciation Monitor (ACSM) for routine monitoring of the composition and mass concentrations of ambient aerosol, Aerosol Sci. Tech., 45, 780–794, 2011.

Onasch, T. B., Trimborn, A., Fortner, E. C., Jayne, J. T., Kok, G. L., Williams, L. R., Davidovits, P., and Worsnop, D. R.: Soot particle aerosol mass spectrometer: development, validation, and initial application, Aerosol Sci. Tech., 46, 804–817, 2012.

Pagels, J., Dutcher, D. D., Stolzenburg, M. R., McMurry, P. H., Gaelli, M. E., and Gross, D. S.: Fine-particle emissions from solid biofuel combustion studied with single-particle mass spectrometry: identification of markers for organics, soot, and ash components, J. Geophys. Res.-Atmos., 118, 859–870, 2013.

Rebotier, T. P. and Prather, K. A.: Aerosol time-of-flight mass spectrometry data analysis: a benchmark of clustering algorithms, Anal. Chim. Acta, 585, 38–54, 2007.

Reilly, P. T. A., Lazar, A. C., Gieray, R. A., Whitten, W. B., and Ramsey, J. M.: The elucidation of charge-transfer-induced matrix effects in environmental aerosols via real-time aerosol mass spectral analysis of individual airborne particles, Aerosol Sci. Tech., 33, 135–152, 2000.

ACPD
15, 32157–32183, 2015

Saleh, R., Robinson, E. S., Tkacik, D. S., Ahern, A. T., Liu, S., Aiken, A. C., Sullivan, R. C., Presto, A. A., Dubey, M. K., Yokelson, R. J., Donahue, N. M., and Robinson, A. L.: Brownness of organics in aerosols from biomass burning linked to their black carbon content, Nat. Geosci., 7, 647–650, 2014.

Smith, J. S., Laskin, A., and Laskin, J.: Molecular characterization of biomass burning aerosols using high-resolution mass spectrometry, Anal. Chem., 81, 1512–1521, 2009.

Sun, H., Biedermann, L., and Bond, T. C.: Color of brown carbon: a model for ultraviolet and visible light absorption by organic carbon aerosol, Geophys. Res. Lett., 34, L17813, doi:10.1029/2007GL029797, 2007.

Washenfelder, R. A., Attwood, A. R., Brock, C. A., Guo, H., Xu, L., Weber, R. J., Ng, N. L., Allen, H. M., Ayres, B. R., Baumann, K., Cohen, R. C., Draper, D. C., Duffey, K. C., Edgerton, E., Fry, J. L., Hu, W. W., Jimenez, J. L., Palm, B. B., Romer, P., Stone, E. A., Wooldridge, P. J., and Brown, S. S.: Biomass burning dominates brown carbon absorption in the rural southeastern United States, Geophys. Res. Lett., 42, 653–664, 2015.

Willis, M. D., Lee, A. K. Y., Onasch, T. B., Fortner, E. C., Williams, L. R., Lambe, A. T., Worsnop, D. R., and Abbatt, J. P. D.: Collection efficiency of the soot-particle aerosol mass spectrometer (SP-AMS) for internally mixed particulate black carbon, Atmos. Meas. Tech., 7, 4507–4516, doi:10.5194/amt-7-4507-2014, 2014.

Willis, M. D., Healy, R. M., Riemer, N, West, M., Wang, J. M., Jeong, C.-H., Wenger, J., Evans, G. J., Abbatt, J. P. D., and Lee, A. K. Y.: Quantification of Black carbon mixing state from traffic: implications for aerosol optical properties, in review, 2015.

ACPD
15, 32157–32183, 2015

Table 1. Summary of LS-SP-AMS single particle cluster analysis.

Particle class	Number of particles	Percentage (%)	Average mass fraction of rBC (mf_{rBC})	Average ion fraction of m/z 39	Average ion fraction of m/z 100–650
SO_4-rich	200	3	0.04	0.01	0.27
NO_3-rich	344	5	0.05	0.02	0.05
rBC-rich	78	1	0.86	0.04	0.07
BBOA-K	1020	15	0.14	0.33	0.02
BBOA-1	872	12	0.03	0.02	0.04
BBOA-2	1645	24	0.03	0.02	0.23
BBOA-3	1956	28	0.03	0.01	0.51
BBOA-4	745	11	0.05	0.01	0.56
Unknown	139	2	–	–	–

ACPD
15, 32157–32183, 2015

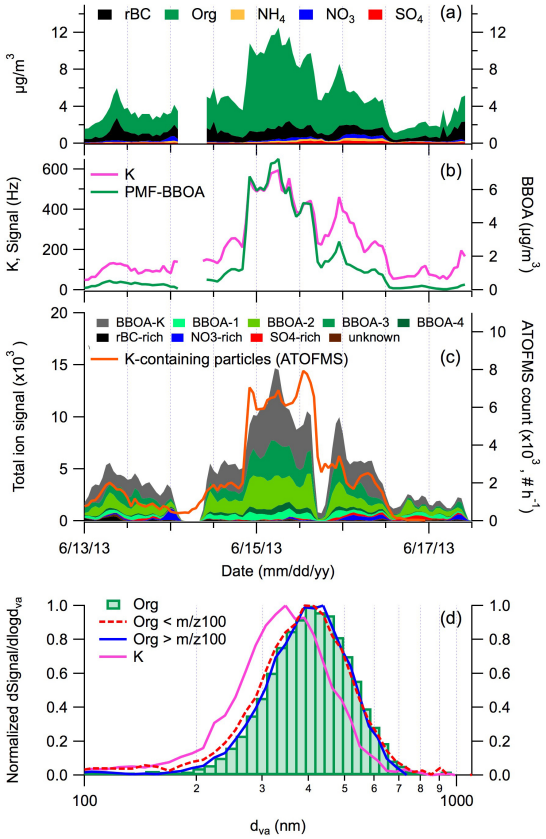

Figure 1. Time series of **(a)** rBC and NR-PM_{rBC} (Org, SO_4, NO_3, NH_4), **(b)** K^+ and PMF-BBOA factor measured by the LS-SP-AMS, **(c)** number of K-containing particles measured by the ATOFMS (right axis) and total ion signal of all particle classes identified by cluster analysis of LS-SP-AMS data (left axis). **(d)** Size distributions of K^+ and Org associated with rBC measured by the LS-SP-AMS.

ACPD
15, 32157–32183, 2015

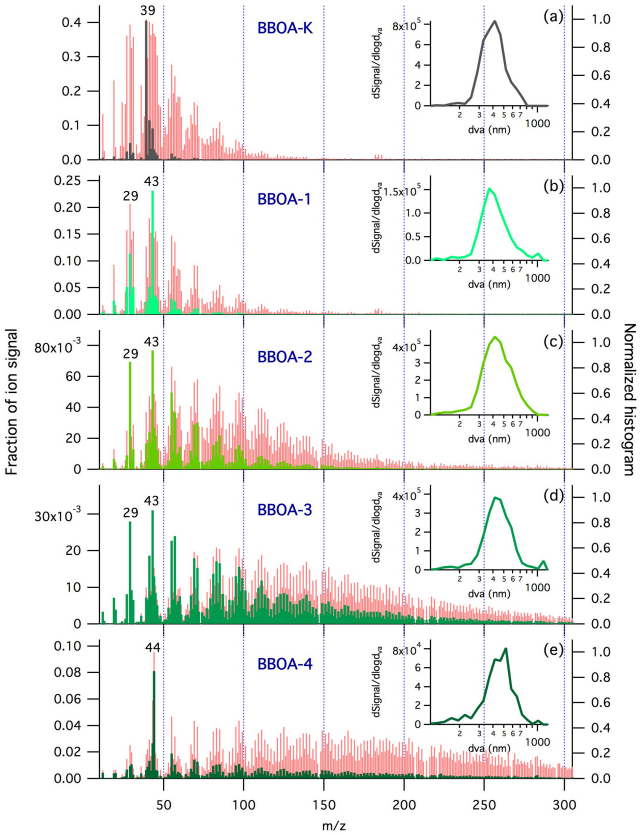

Figure 2. Average mass spectra (left axis), normalized mass spectral histograms (showing the relative frequency of a signal at each m/z, right axis), and size distributions (insets) of the five BBOA-related particle classes identified by cluster analysis of LS-SP-AMS data.

ACPD
15, 32157–32183, 2015

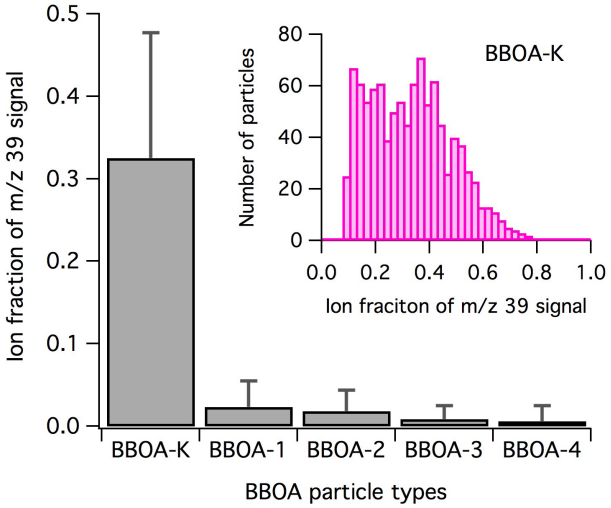

Figure 3. Ion fraction of m/z 39 signal (a tracer of K^+) for each BBOA-related particle class. Histogram of the ion fraction of m/z 39 for the BBOA-K particle class (inset).

ACPD
15, 32157–32183, 2015

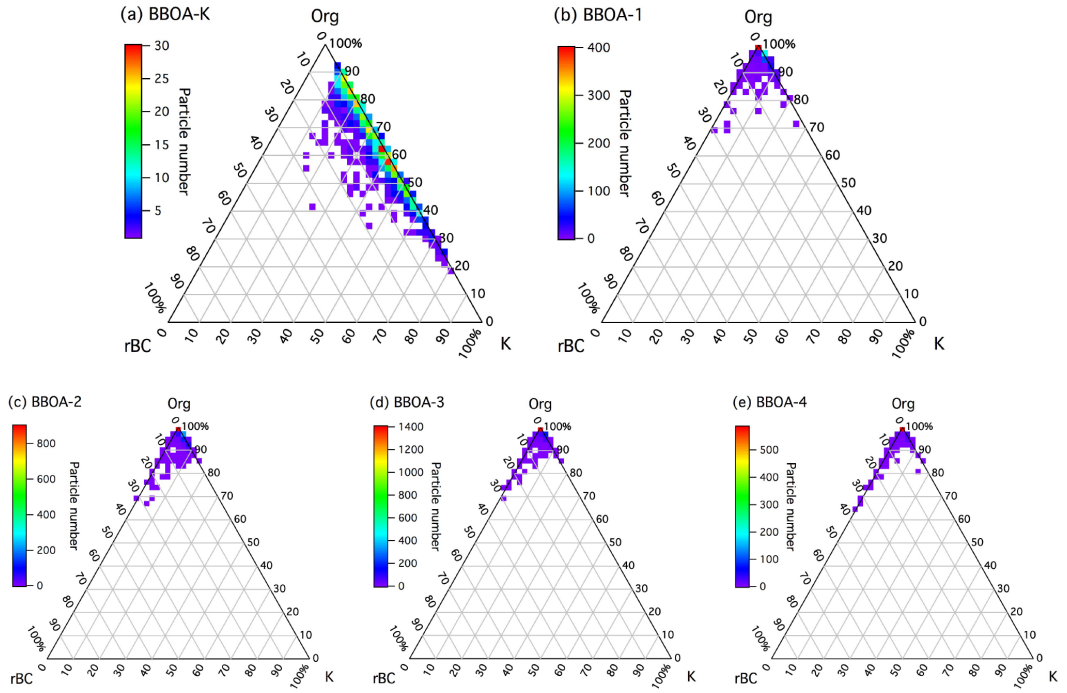

Figure 4. Ternary plots of rBC, Org_{BC} and K ion signal for the five BBOA particle types.

ACPD
15, 32157–32183, 2015

Single particle characterization of biomass burning organic aerosol (BBOA)

A. K. Y. Lee et al.

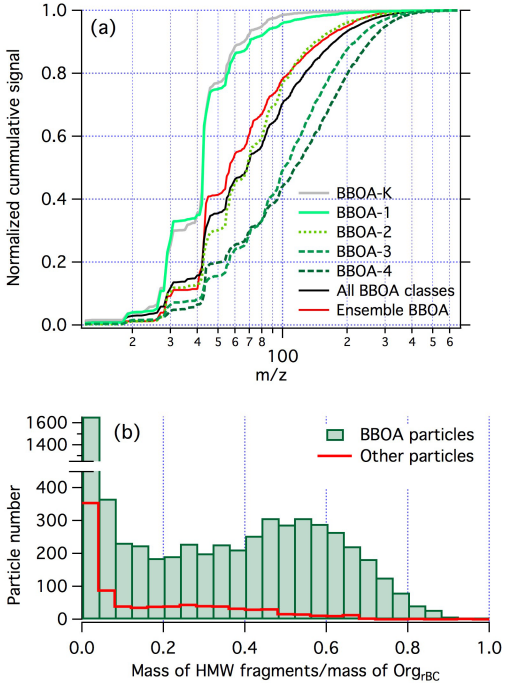

Figure 5. (a) Normalized cumulative histogram of mass-to-charge ratios for each BBOA-related particle class. **(b)** Histograms of the mass fraction of HMW organic fragments (> m/z 100) in different particle types.

ACPD
15, 32157–32183, 2015

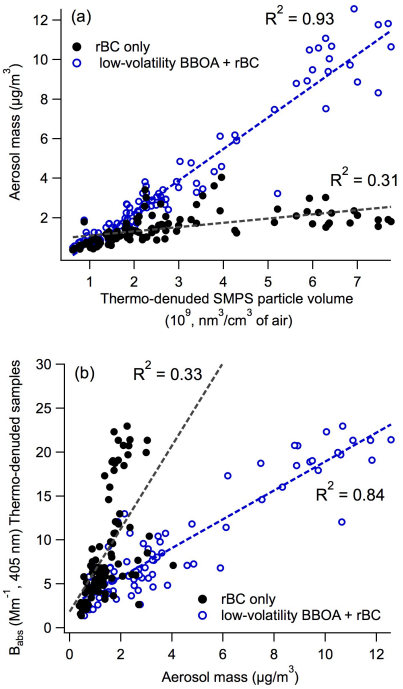

Figure 6. (a) Correlation of the estimated total of non- and low-volatility aerosol mass (rBC + 60 % of the total BBOA) and thermo-denuded particle volume measured by the SMPS. **(b)** Correlations of aerosol absorption at 405 nm of thermo-denuded particles (B_{abs}) and the estimated total of non- and low-volatility aerosol mass.

ACPD
15, 32157–32183, 2015